background image : NGC 6139

Journal Club 06:

Origin of neutron-capture elements with the Gaia-ESO survey: the evolution of s- and r-process elements across the Milky Way
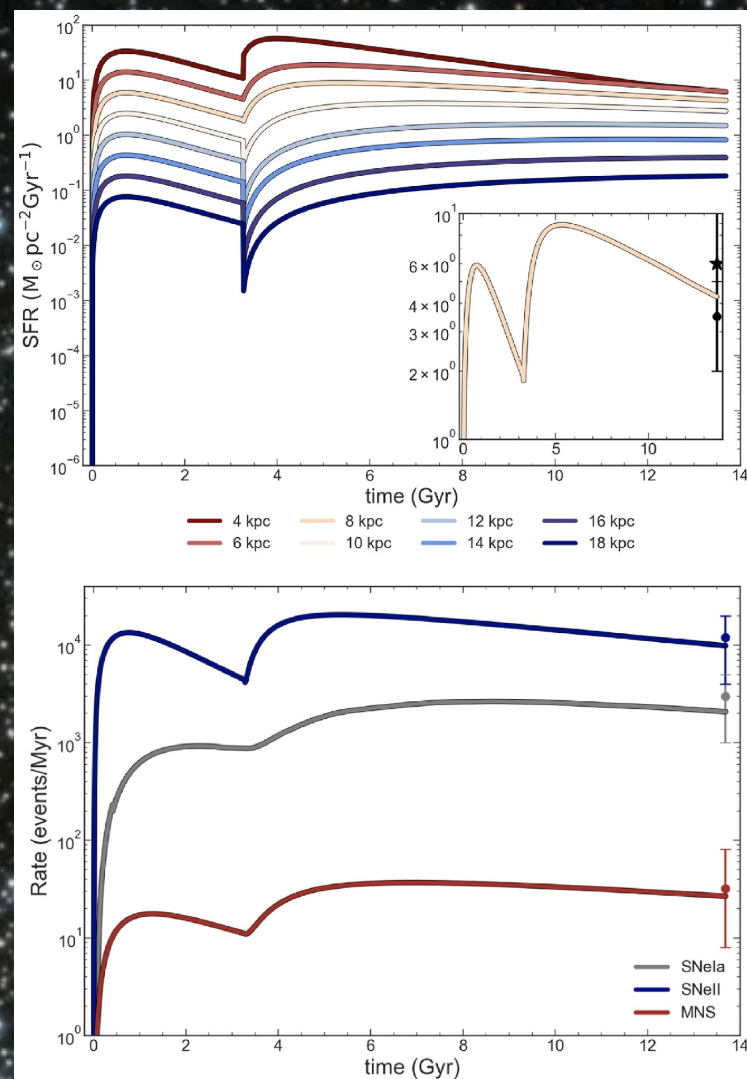
ABSTRACT

We investigate the origin of neutron-capture elements by analysing their abundance patterns and radial gradients in the Galactic thin disc. We adopt a detailed two-infall chemical evolution model for the Milky Way, including state-of-the-art nucleosynthesis prescriptions for neutron-capture elements. We consider r-process nucleosynthesis from merging neutron stars (MNS) and magneto-rotational supernovae (MR-SNe), and s-process synthesis from low- and intermediate-mass stars (LIMS) and rotating massive stars. The predictions of our model are compared with data from the sixth data release of the *Gaia*-ESO survey, from which we consider 62 open clusters with age $\gtrsim 0.1$ Gyr and $\sim$1300 Milky Way disc field stars. We conclude that: (i) the [Eu/Fe] versus [Fe/H] diagram is reproduced by both prompt and delayed sources, with the prompt source dominating Eu production; (ii) rotation in massive stars significantly contributes to the first peak s-process elements, but MNS and MR-SNe are necessary to match the observations; and (iii) our model slightly underpredicts Mo and Nd, while accurately reproducing the [Pr/Fe] versus [Fe/H] trend. Regarding the radial gradients, we find that: (i) our predicted [Fe/H] gradient slope agrees with observations from *Gaia*-ESO and other high-resolution spectroscopic surveys; (ii) the predicted [Eu/H] radial gradient slope is steeper than the observed one, regardless of how quick the production of Eu is, prompting discussion on different Galaxy-formation scenarios and stellar radial migration effects; and (iii) elements in the second s-process peak as well as Nd and Pr exhibit a plateau at low-Galactocentric distances, likely due to enhanced enrichment from LIMS in the inner regions.
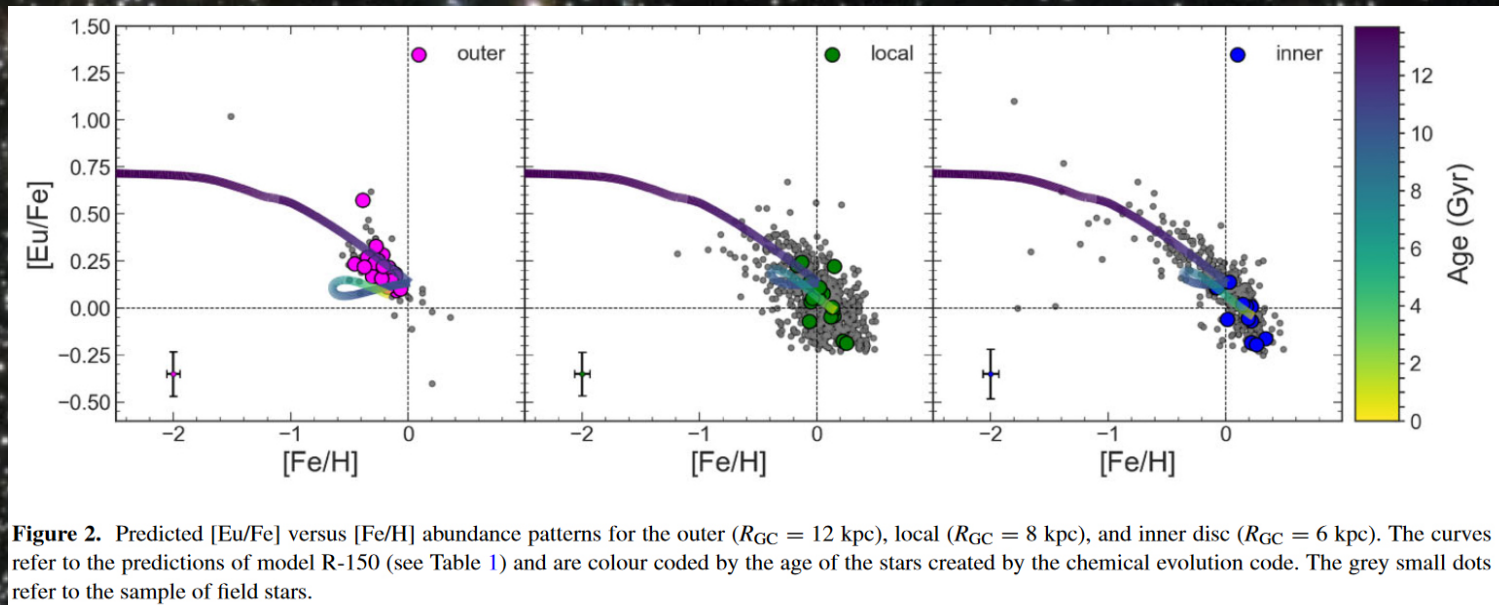
Key words: nuclear reactions, nucleosynthesis, abundances – stars: neutron – stars: rotation – supernovae: general – Galaxy: abundances – Galaxy: evolution.

Table 1. Nucleosynthesis prescriptions. In the 1st column we report the name of the model, in the 2nd the initial rotational velocities for massive stars. In the 3rd, 4th, and 5th columns we list whether LIMS, MR-SNe, and MNS channels are active or not, respectively. We point out that in the case of model 'R-150 MNS' MNS are assumed to merge with a short and constant time delay of 10 Myr instead that with a DTD.

Model	v_{MS} (km s^{-1})	LIMS	MR-SNe	MNS
R-0	0	✓	✓	✓
R-150	150	✓	✓	✓
R-300	300	✓	✓	✓
R-150 MNS	150	✓	X	✓
R-150 MRD	150	✓	✓	X
noR-0	0	✓	X	X
noR-150	150	✓	X	X
noR-300	300	✓	X	X

- Upper panel: time evolution of the SFR as predicted by our models at various Galactocentric distances.

- Right corner plot: Predicted SFR in the solar neighbourhood compared with present-day estimates (Guesten & Mezger 1982; P18).

- Lower panel: Predicted SNeIa, SNeII, and MNS rates compared with present-day observations from Cappellaro, Evans & Turatto (1999; for SNe) and estimate from Abbott et al. (2021; for MNS).

Figure 2. Predicted [Eu/Fe] versus [Fe/H] abundance patterns for the outer ($R_{GC} = 12$ kpc), local ($R_{GC} = 8$ kpc), and inner disc ($R_{GC} = 6$ kpc). The curves refer to the predictions of model R-150 (see Table 1) and are colour coded by the age of the stars created by the chemical evolution code. The grey small dots refer to the sample of field stars.

- **Yttrium: 78% s-process**

- **Barium: 89% s-process**

- **Zirconium: 82% s-process**

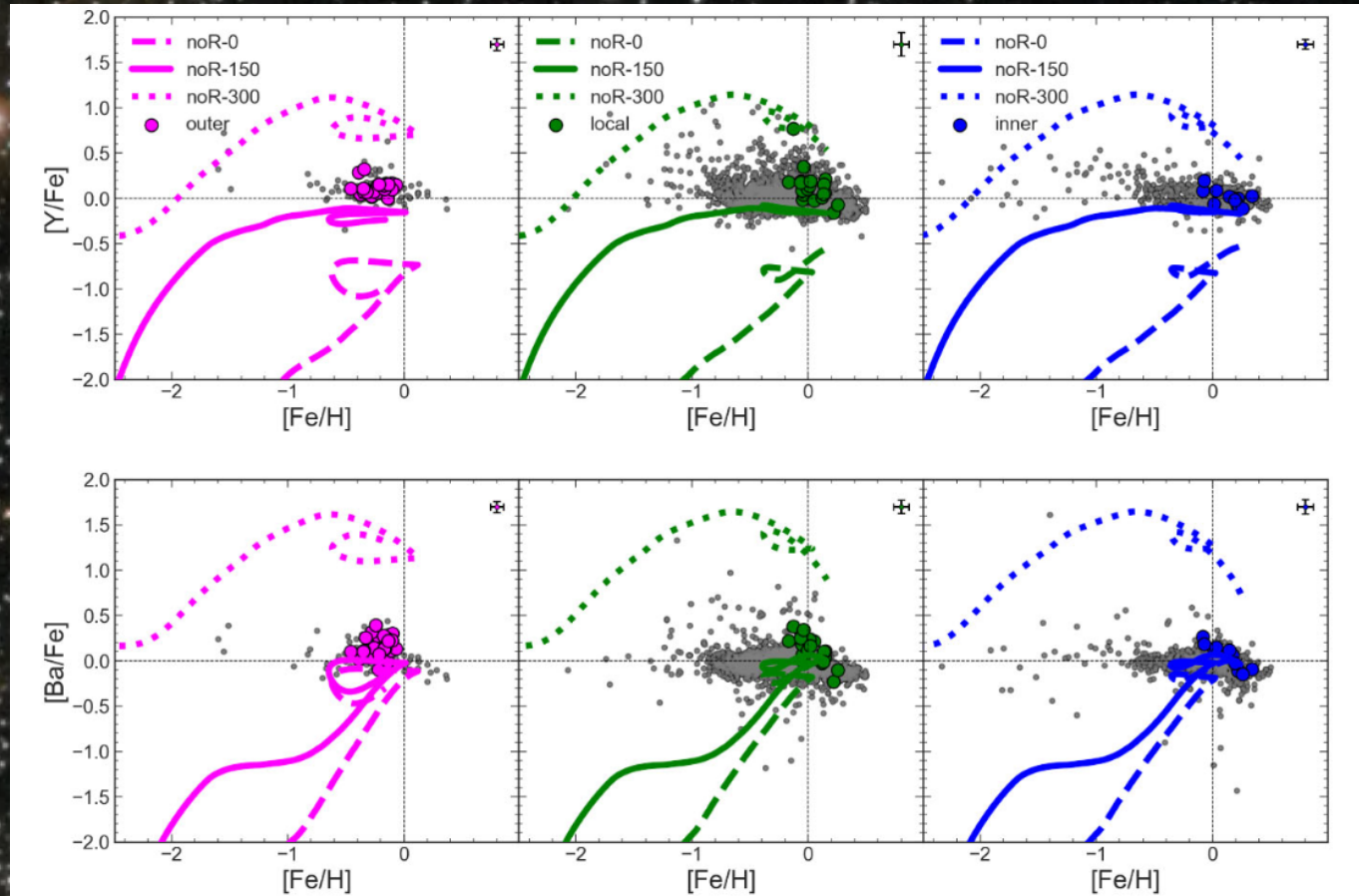- **Lanthanum: 80% s-process**

- **Cerium: 85% s-process**

Figure 4. Predicted abundance patterns for [Y/Fe] and [Ba/Fe] versus [Fe/H] for outer-disc ($R_{GC} = 12$ kpc), local-disc ($R_{GC} = 8$ kpc), and inner-disc ($R_{GC} = 6$ kpc) regions. We assume that only massive stars and LIMS are Y and Ba producers. The three lines in each plot correspond to different initial rotational velocities of massive stars (see legend and Table 1).
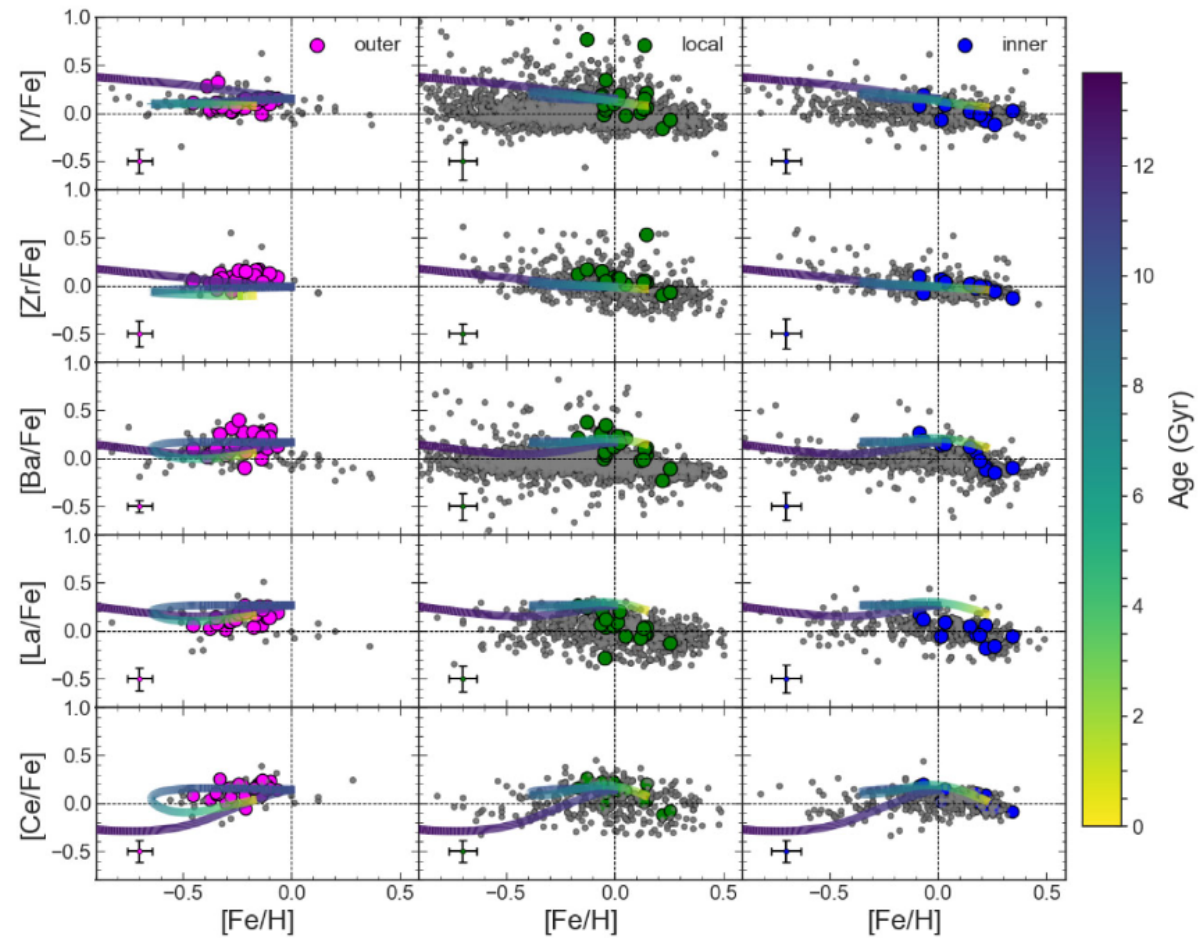
Figure 5. Predictions from model R-150 for the s-process elements abundance patterns versus [Fe/H] for outer-disc ($R_{GC} = 12$ kpc), local-disc ($R_{GC} = 8$ kpc), and inner-disc ($R_{GC} = 6$ kpc) regions. The channels considered for the production of the s-process components are: massive stars with initial rotational velocities of 150 km s^{-1} and LIMS. The channels for the r-process components are: MR-SNe and MNS with a DTD. The curves are colour coded by the age of the stars created by the chemical evolution code.

- **Molybdenum: around 50% s-process, 27% r-process and 23% p-process.**

- **Neodymium: around 40% r-process.**
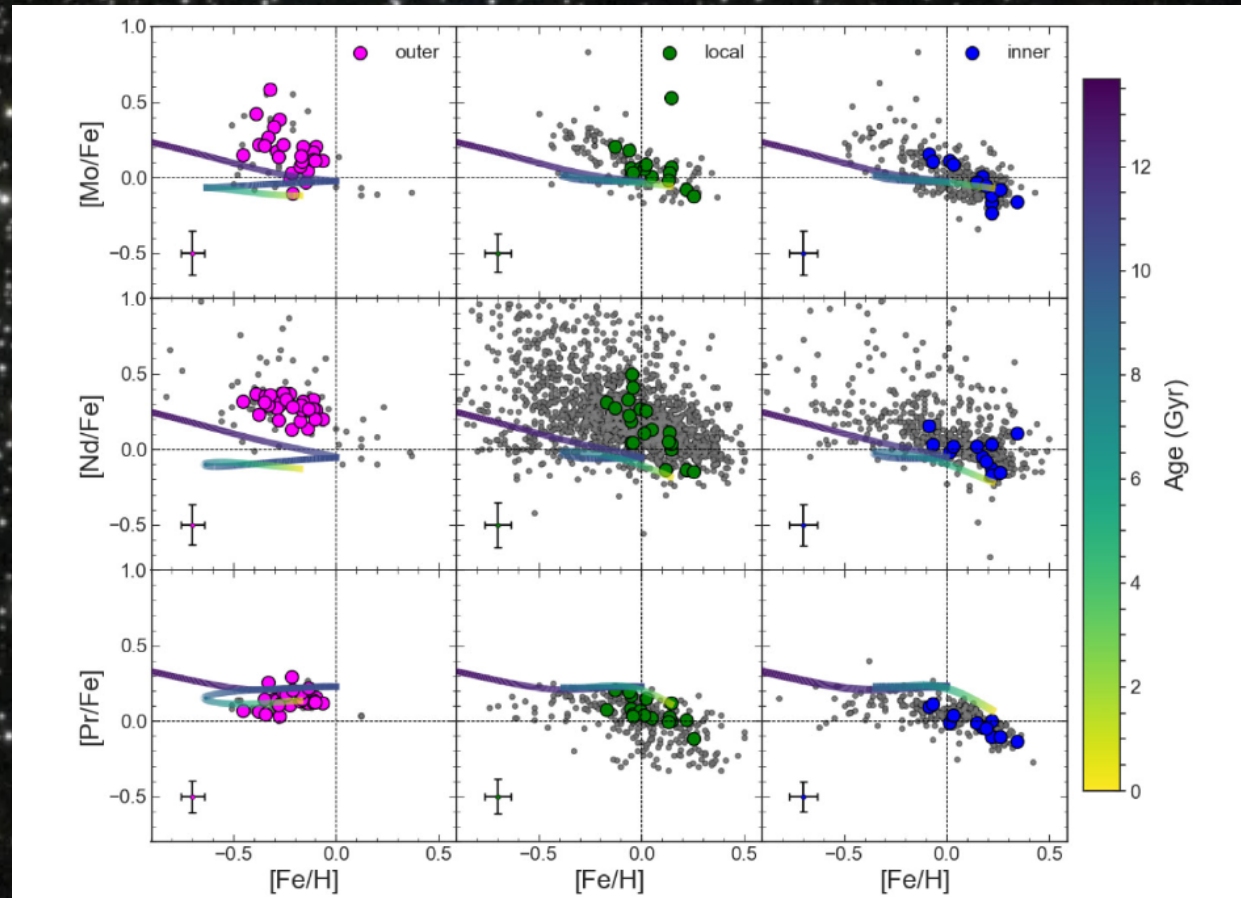
- **Praseodymium: around 50% r-process.**

Figure 6. Predictions from model R-150 for the mixed-process elements abundance patterns versus [Fe/H] for outer-disc (R_{GC} = 12 kpc), local-disc (R_{GC} = 8 kpc), and inner-disc (R_{GC} = 6 kpc) regions. The curves are colour coded by the age of stars created by the chemical evolution code.
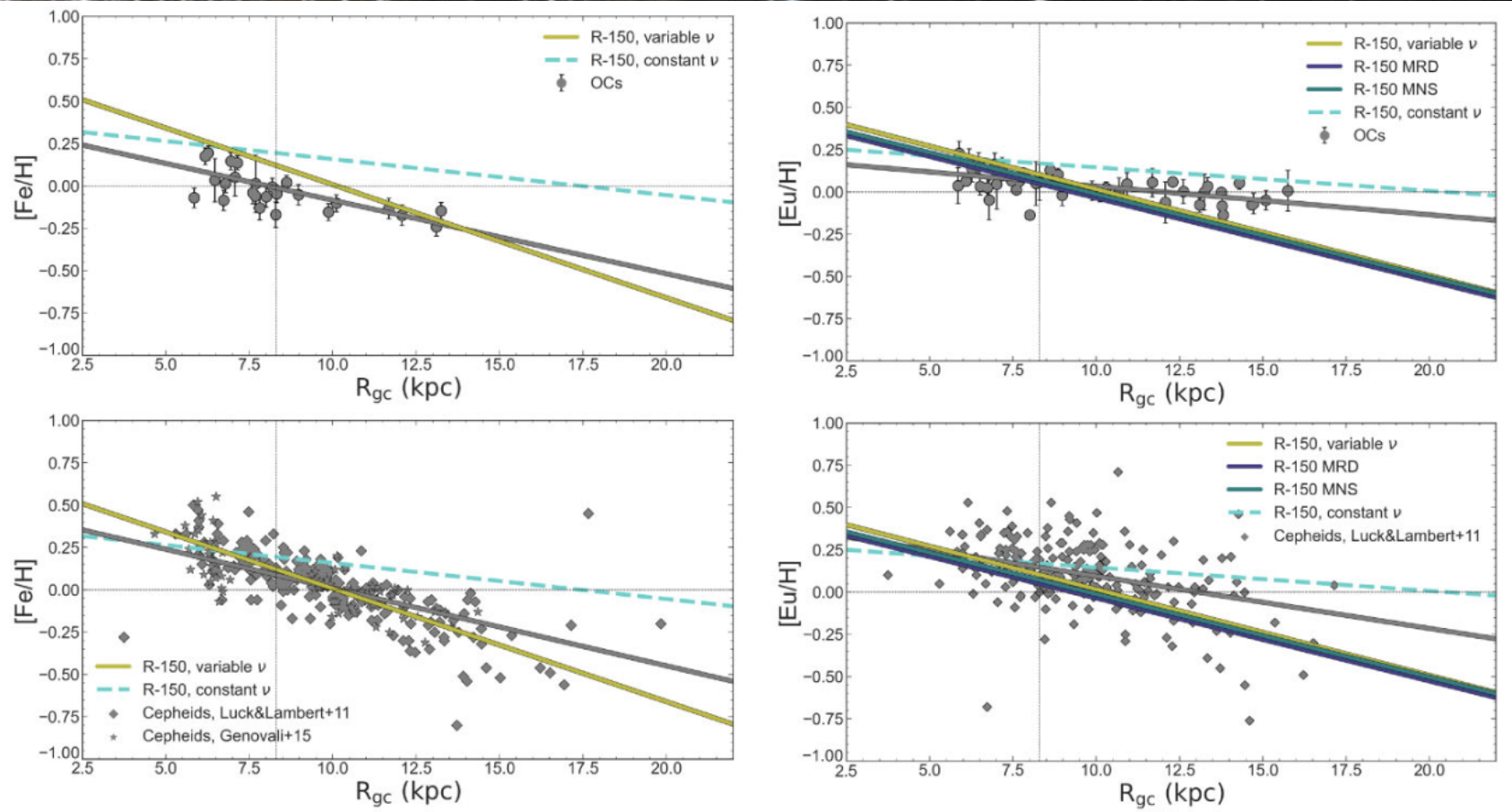
Figure 7. Prediction of the present-day slope of the [Fe/H] and [Eu/H] gradients from our models with variable (olive line) and constant (dashed turquoise line) SF efficiency compared with the one of the restricted (age ≤ 3 Gyr) OC sample (upper panel) and the Cepheid sample (lower panel) with data from Luck & Lambert (2011) (grey diamonds) and Genovali et al. (2015) (grey stars). For the [Eu/H], we show also models with Eu produced only by MR-SNe (purple line) and Eu produced only by MNS with a constant and short delay time for merging (teal line). The grey lines represent the linear fit of the observational data.

Table 2. Slopes of the [Fe/H] and [Eu/H] gradients of the reduced (Age ≤ 3 Gyr) OC sample and as predicted by our model for the all, inner (R_{GC} < 11.2 kpc) and outer (R_{GC} > 11.2 kpc) radial region. For comparison we show also the one obtained from the Cepheid sample of Luck & Lambert (2011) and Genovali et al. (2015). In the case of Eu we show predictions also of models in which Eu is produced either by MR-SNe or by MNS with a constant and short delay time for merging.

	[Fe/H]			[Eu/H]		
	m_{tot} (dex kpc^{-1})	m_{inner} (dex kpc^{-1})	m_{outer} (dex kpc^{-1})	m_{tot} (dex kpc^{-1})	m_{inner} (dex kpc^{-1})	m_{outer} (dex kpc^{-1})
OCs	-0.049 ± 0.005	-0.081 ± 0.013	-0.045 ± 0.017	-0.017 ± 0.003	-0.024 ± 0.009	-0.015 ± 0.014
Cepheids	-0.046 ± 0.003	–	–	-0.031 ± 0.004	–	–
Model R-150 var ν	-0.067 ± 0.002	-0.064 ± 0.008	-0.063 ± 0.007	-0.051 ± 0.003	-0.038 ± 0.004	-0.057 ± 0.007
Model R-150 con ν	-0.021 ± 0.004	-0.044 ± 0.008	-0.007 ± 0.001	-0.014 ± 0.003	-0.029 ± 0.006	-0.004 ± 0.001
Model R-150 MRD	–	–	–	-0.049 ± 0.003	-0.034 ± 0.003	-0.057 ± 0.007
Model R-150 MNS	–	–	–	-0.049 ± 0.003	-0.034 ± 0.003	-0.057 ± 0.007

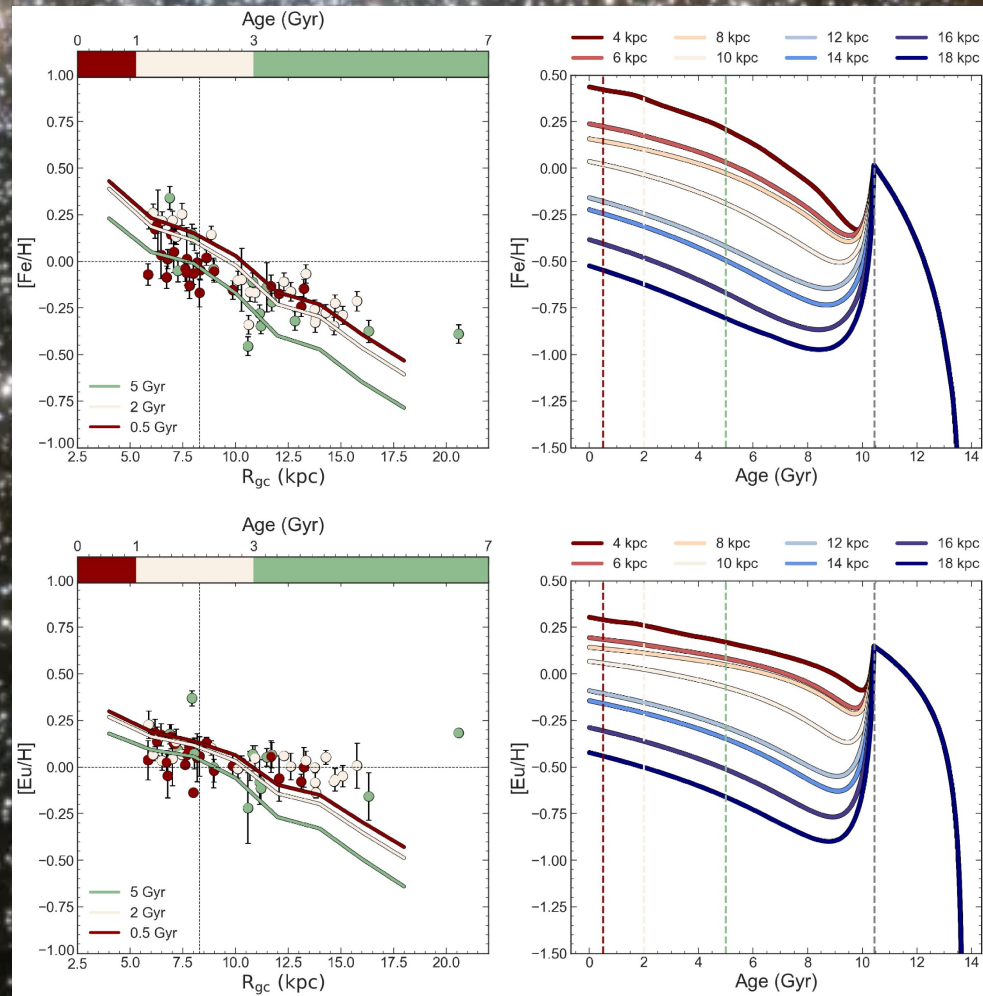**Figure 8.** Left-hand panels: Time evolution of the radial [Fe/H] and [Eu/H] gradients as predicted by model R-150. The OC sample is divided in three age bins: young (age < 1 Gyr), intermediate (1 < age < 3 Gyr), and old (age > 3 Gyr). Solid lines are the results for the [Fe/H] gradient as predicted by our model at 0.5, 2, and 5 Gyr. Right-hand panel: Time evolution of the [Fe/H] and [Eu/H] as predicted by model R-150 for different Galactocentric distances. Vertical dotted lines indicate the ages considered to compute the gradients.
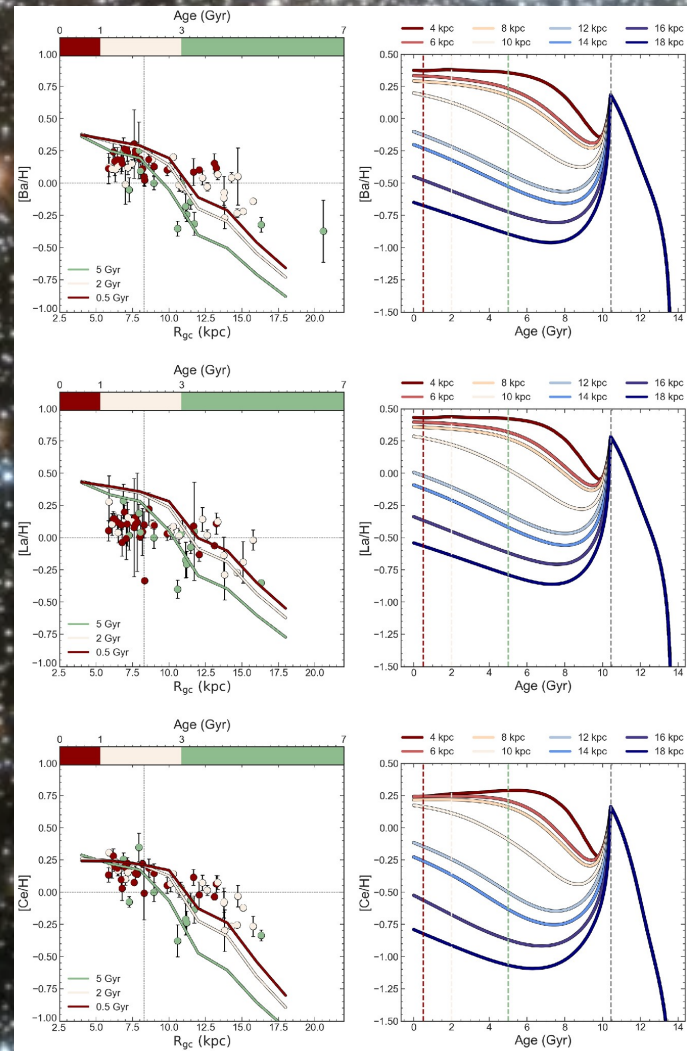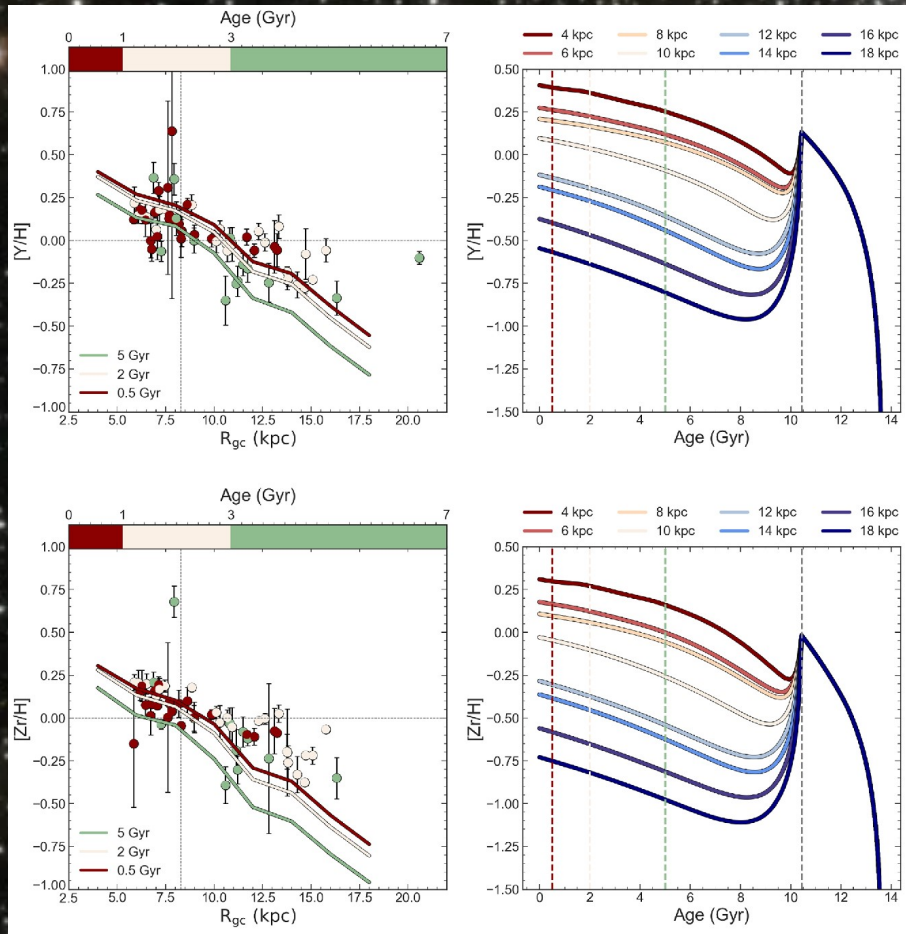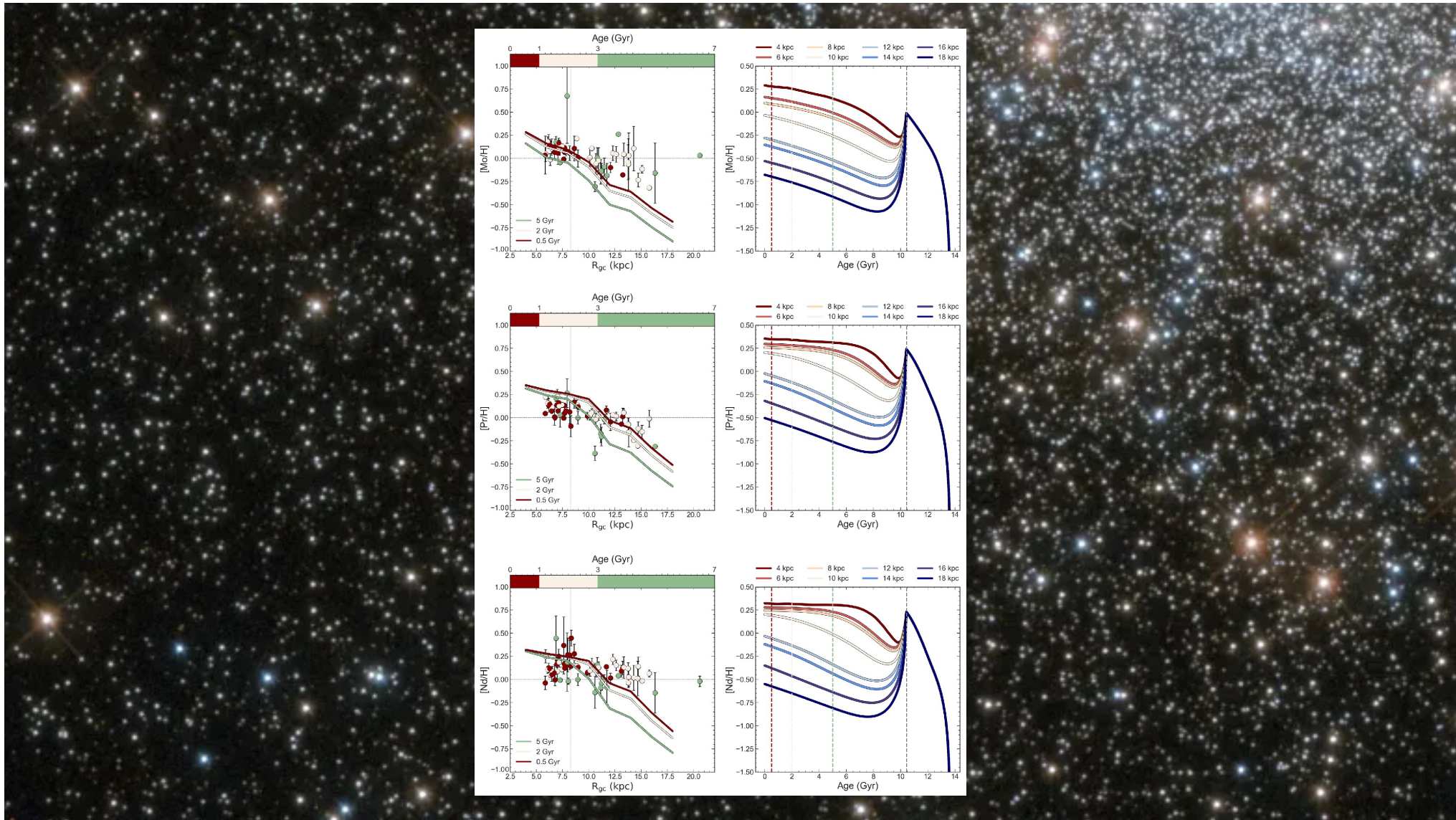
Table 3. Slopes of the [El/H] gradients predicted by our model at age = 0.5, 2, and 5 Gyr.

	Age = 0.5 Gyr	Age = 2 Gyr	Age = 5 Gyr
[Fe/H]	-0.067 ± 0.002	-0.069 ± 0.002	-0.073 ± 0.003
[Eu/H]	-0.051 ± 0.003	-0.053 ± 0.004	-0.059 ± 0.004
[Y/H]	-0.067 ± 0.004	-0.070 ± 0.004	-0.077 ± 0.005
[Zr/H]	-0.075 ± 0.004	-0.078 ± 0.004	-0.083 ± 0.004
[Ba/H]	-0.078 ± 0.008	-0.084 ± 0.007	-0.095 ± 0.006
[La/H]	-0.073 ± 0.008	-0.080 ± 0.007	-0.092 ± 0.006
[Ce/H]	-0.077 ± 0.011	-0.087 ± 0.011	-0.105 ± 0.008
[Mo/H]	-0.071 ± 0.003	-0.073 ± 0.003	-0.077 ± 0.004
[Pr/H]	-0.078 ± 0.012	-0.089 ± 0.012	-0.109 ± 0.009
[Nd/H]	-0.058 ± 0.004	-0.062 ± 0.004	-0.070 ± 0.005

CONCLUSIONS

- The [Eu/Fe] versus [Fe/H] abundance pattern is well reproduced if both a quick source and a delayed one act as r-process producers. With the assumed prescriptions the quick source completely dominates the production of Eu. However, since MNS are the only observed source of neutron-capture elements up to now, they cannot be excluded from chemical evolution models computations.

- The s-process elements' abundances pattern is not reproduced if one considers only production from typical s-process astrophysical sources as rotating massive stars and LIMS. Rotation increases the production of s-process material, especially at low metallicities and for elements belonging to the first s-process peak, but the r-process component must also be taken into account.

- When adding the contribution from MNS and MR-SNe to the production of the r-process component of the s-process elements, MR-SNe dominate at low metallicities and it is no longer possible to appreciate differences between different rotational velocities for massive stars. The s-process abundance pattern of the OC sample is well reproduced.

- The picture for the mixed-/r-process elements is more complex. A good agreement with the relevant data is obtained for Mo, even if the model still slightly underestimates the observations, most probably because of the lack of an additional contribution from neutrino-driven SNe. For Nd and Pr, our model shows a higher production from LIMS of Pr than of Nd. Also in this case, the model underproduces the [Nd/Fe] versus [Fe/H] abundance pattern, while nicely reproduces the [Pr/Fe] versus [Fe/H] one.

CONCLUSIONS

- The present-day slope of the [Fe/H] gradient predicted by our model is slightly steeper both with respect to that of the restricted OC sample and to the one of the Cepheid sample, yet it agrees with other recent slopes of the [Fe/H] gradient from OC samples (Carrera et al. 2019; Donor et al. 2020; Spina et al. 2021, 2022; Zhang et al. 2021).

- The flat slope observed in the OC sample for [Eu/H] is not reproduced by the model in which Eu is produced by a quick and a delayed source. Models with no delayed source do not improve the fit to the data. We discussed the possibility of flattening the predicted [Eu/H] gradient by adopting a constant SF efficiency. However, we are not inclined to relax the assumption of a variable SF efficiency since it has already been proved hat the inside-out scenario by itself is not able to explain the abundance patterns at different Galactocentric distances and the abundance gradients for several elements, as well as the gradient of the SFR and gas density along the thin disc. A reasonable explanation for the discrepancy between model results and observations could thus be that clusters with intermediate age (1 ≤ age ≤ 3 Gyr) are affected by radial migration. In favour of this hypothesis, predictions of our model are much more in agreement with the slopes observed in the inner disc rather than with the outer ones and a better agreement is also obtained with the radial gradients of the Cepheid sample.

- Regarding the time evolution of the [Fe/H] gradient, results of our model for age = 0.5, 2, and 5 Gyr are in agreement with the observed trend if the gradient of the youngest population is computed by removing all giant stars with logg < 2.5. In particular, a really limited time evolution of the [Fe/H] gradient between the considered ages should be expected.

CONCLUSIONS

- Also for the [Eu/H] gradients, a limited evolution with time is predicted by our model, in agreement with the observations. However, as already seen in the case of the present-day gradient also at different ages, we obtain slopes which are too steep with respect to the observations.

- Predictions of our model for the radial [Y/H] and [Zr/H] gradients show a very similar pattern for age = 0.5 and 2 Gyr, in agreement with the OC sample. Also in the case of Ba, La, and Ce, the model predicts an almost identical flat or slightly decreasing pattern for all ages in the inner zone, as observed in the OC sample.

- As for the abundance patterns, also for the radial gradients much more uncertainty is present in reproducing the trend of the other mixed-/r-process elements. Due to the adopted nucleosynthesis prescriptions, we underestimate the trends for Mo and Nd, and always produce steeper gradients with respect to the observed ones.

- For all the elements belonging to the second s-process peak as well as for Nd and Pr, our model produces a plateau for low Galactocentric distances at all the considered ages. This is most probably due to the effect of LIMS, whose production of those elements reaches an equilibrium value before that in the outer regions, as a consequence of a faster SF.

MODEL

$$\dot{G}_i(R, t) = -\Psi(R, t)X_i(R, t) + R_i(R, t) + \dot{G}_{i,\text{inf}}(R, t).$$

$$\dot{G}_{i,\text{inf}}(R, t) = A(R)X_{i,\text{inf}}e^{-t/\tau_1} + \theta(t - t_{\text{max}})B(R)X_{i,\text{inf}}e^{-(t-t_{\text{max}})/\tau_2},$$

$$\tau_2(R) = \left(1.033\frac{R}{\text{kpc}} - 1.267\right) \text{Gyr.}$$

DATA SAMPLE

- We consider among the sample of OCs observed by Gaia-ESO, the 62 clusters older than 100 Myr, as done in M23. The distribution in age and distances of our sample OCs is given in Viscasillas V´azquez et al. (2022, see their fig. 1). For each cluster, we considered the average abundances of its member stars.

- In the paper, we use the OC sample to trace the abundance radial gradients, and thanks to the wide age range, also their evolution over time.

- The sample of field stars is composed, as in Viscasillas V´azquez et al. (2022). We combined the two samples, applying a further selection on the signal-to-noise ratio (SNR) and on the uncertainties on the stellar parameters: SNR > 20; σ Teff < 150 K, σ log g < 0.25, σ [Fe/H] < 0.20, and σ ξ < 0.20 km s^{-1}. A final selection was introduced considering only stars with at least one measurement of the abundances of one of the considered neutron-capture elements, and with an uncertainty eA(El) < 0.1.